PERGAMON

Engineering Fracture Mechanics 70 (2003) 1245–1257

Engineering Fracture Mechanics

www.elsevier.com/locate/engfracmech

Experimental analysis of the practical LBZ effects on the brittle fracture performance of cryogenic steel HAZs with respect to crack arrest toughness near fusion line

Jae-il Jang [a,*], Baik-Woo Lee [b], Jang-Bog Ju [b], Dongil Kwon [b], Woo-sik Kim [c]

[a] *Frontics, Inc., Research Institute of Advanced Materials, Seoul National University, Seoul 151-742, South Korea*
[b] *School of Materials Science and Engineering, Seoul National University, Seoul 151-742, South Korea*
[c] *Research and Development Center, Korea Gas Corporation, Ansan 425-150, South Korea*

Received 1 November 2001; received in revised form 14 May 2002; accepted 5 June 2002

Abstract

Focusing on crack arrest behavior, this study investigates the practical influence of local brittle zones (LBZs) on the brittle fracture resistance of heat-affected zones (HAZs) in advanced 9% Ni cryogenic steel welds, and discusses whether the LBZs of this steel in practice have potentially deleterious effects as previously thought, or not. By analyzing the variations in brittle crack arrest toughness (K_a) and brittle crack initiation toughness (K_c) within actual HAZ, it is found that LBZs of this steel may not be harmful in consideration of crack arrest toughness near fusion line.

Keywords: Local brittle zones; Heat-affected zones; Crack arrest; Crack tip opening displacement; 9% Ni cryogenic steel

1. Introduction

It is now widely recognized that small zones exhibiting abnormally poor fracture resistance, referred to as local brittle zones (LBZs), can exist in the heat-affected zones (HAZs) of multi-pass welded structural steel. Since research on LBZs began, LBZs have been found to cause low toughness values in various toughness tests such as the Charpy impact test and the crack tip opening displacement (CTOD) test and to reduce the resistance to brittle fracture initiation [1–6]. Based upon these studies, some industry standards, such as API RP 2Z [7] and EEMUA 150 [8], have been established containing, in some form, a requirement that certain HAZ CTOD specimens must sample at least 15% of the coarse-grained HAZ (CGHAZ) microstructure. With a similar viewpoint, the LBZ phenomena of the quenching, larmellarizing and tempering (QLT)-processed 9% Ni steels, which have been newly developed and currently used for the inner walls of large-scale liquefied natural gas (LNG) storage tanks due to enhanced cryogenic toughness at, or below, LNG temperature of 111 K [9], were observed and analyzed in the authors' previous studies [10,11]. In the

* Corresponding author. Tel.: +82-2-884-8025; fax: +82-2-889-4380.
E-mail address: jijang@frontics.com (J.-i. Jang).

0013-7944/03/$ - see front matter © 2002 Elsevier Science Ltd. All rights reserved.
doi:10.1016/S0013-7944(02)00111-X

studies using the simulated HAZ specimens and K-grooved HAZ specimens, it was found that the intercritically reheated CGHAZ (IC CGHAZ) and unaltered CGHAZ (UA CGHAZ) were primary and secondary LBZs of the steel respectively at LNG temperature.

Like the investigation, steel manufacturers have been performing extensive research on the LBZ phenomena of various structural steel. Paradoxically, however, LBZs have not been reported as a significant cause of failure in practical welded structures, indicating that such a crack-initiation-based assessment of LBZ effects may be a somewhat conservative method for evaluating the practical safety performance of welded structures. With this viewpoint, some researchers have suggested the conservatism of the "crack initiation prevention" approach in relation to the "prevention of crack propagation" approach, although there has been little experimental verifications or systematic identification [12]. Given these research uncertainties, the present work was undertaken to clarify experimentally the practical significance of LBZs on the brittle fracture resistance of the QLT-9% Ni steel at LNG temperature with an emphasis on the crack arrest behavior of weld HAZ.

First, the change in crack arrest toughness within the HAZ including LBZs was evaluated through compact crack arrest (CCA) tests. A second aspect of the present study was to make a direct comparison between the arrest toughness and the crack initiation toughness obtained from CTOD tests in order to discuss the practical influence of LBZs on the brittle fracture performance of the weld HAZ. It is of relevance to note that few studies have shown the experimental results of crack arrestability variation within HAZs, and furthermore until now systematic and experimental analyses of practical LBZ effects through the direct comparison of crack arrest toughness and crack initiation toughness have not been carried out.

2. Experimental procedures

The 9% Ni steel used in this study is a commercial grade used for LNG storage tanks, whose chemical composition is 0.066C–0.24Si–0.65Mn–0.005P–0.005S–9.28Ni. The steel plates are normally processed by the QLT (Q: 1093 K for 60 min, quench, L: 963 K for 80 min, quench, and T: 853 K for 60 min, quench) heat treatment. The QLT process, originally developed for lower Ni steel such as 5.5% Ni steel [13], enhances cryogenic toughness considerably compared to other conventional processes such as quenching and tempering (QT) or double normalizing and tempering (NNT) processes due to the increased amount of stable austenite and the refinement of effective grain size.

The steel plates with 20 mm thickness were machined into X-groove configuration and welded along transverse-to-rolling direction by shielded metal arc welding (SMAW) or submerged arc welding (SAW) processes. Welding was carried out under the same conditions as those used during the construction of the tanks in Korea. Table 1 lists the used welding condition. No significant defects were found in the completed weldments by non-destructive X-ray examination.

To assess the crack arrest toughness, CCA tests were conducted at the LNG temperature of 111 K, in accordance with ASTM E1221 [14]. The CCA test has many advantages compared with other crack arrest toughness testing methods in the use of large-scale specimens: namely, (1) the testing procedure has been standardized [14] unlike most of the other crack arrest tests, (2) the notch location within the HAZ can be easily selected by introducing a side-groove in CCA specimens, (3) unlike the double cantilever beam (DCB)

Table 1
Welding conditions used in this study

Welding method	Filler metal	Polarity	Current (A)	Voltage (V)	Speed (cm/min)	Heat input (kJ/cm)
SAW (flat)	Inconel	DCEP	320–360	25–28	25–53	Avg.23
SMAW (vertical)	Hastelloy	AC	100–130	20–40	6–20	Avg.28

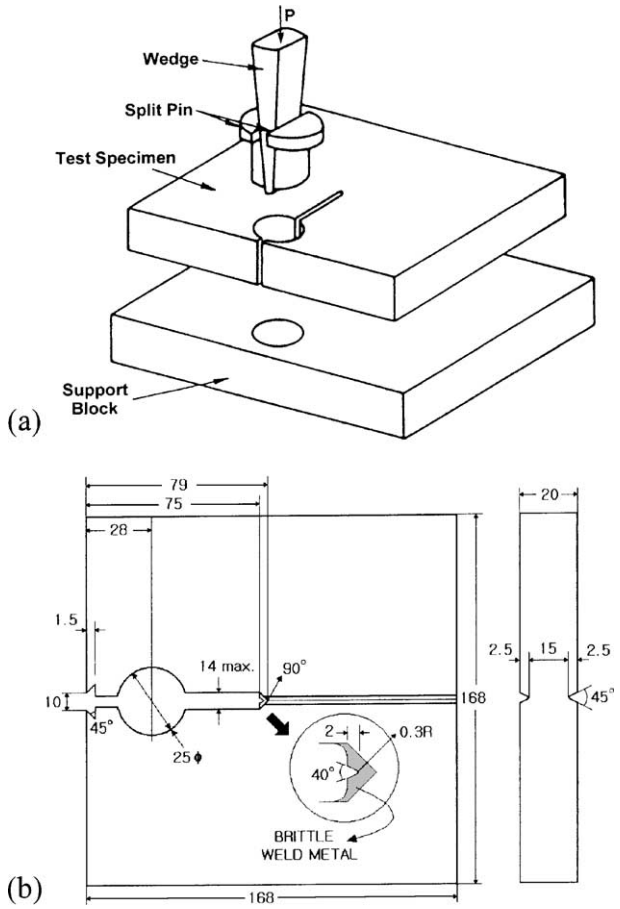

Fig. 1. Schematic views of (a) the arrangement for the CCA test and (b) the geometry of the test specimen.

test using similar-sized specimens, K_a can be evaluated in the CCA test even in the case of $K_a > K_c$, and (4) this test can be conducted economically in the laboratory since it does not require testing machine with a much higher load capacity as is generally needed for such crack arrest tests. Fig. 1 shows the schematic illustration of the test apparatus arrangement and the specimen geometry. The electric discharge machined (EDM) notches in the brittle bead in front of the side grooves were machined at various distances from the fusion line within the HAZ. Both schematic diagram and actual view indicating the change in notch location which is equivalent to side-groove location is shown in Fig. 2.

For measuring crack initiation toughness, the CTOD tests, which have been generally used to evaluate crack initiation fracture toughness of the steel weldments, were performed mainly in accordance with ASTM E1290 and BS 7448 [15,16] at 111 K. Fig. 3 shows the schematic illustration of testing apparatus arrangement and geometry of CTOD specimen used in this study. The through-thickness precrack was also located at a distance from the fusion line of the specimen, and the locations are the same as in Fig. 2(a). When calculating the CTOD values from the crack mouth opening displacement (CMOD) data, the asymmetry of plastic deformation around the crack tip was taken into consideration; consequently, the "local CTOD" concept [17,18] was used because the weldments had strength mismatches between the austenitic weld metal and the ferritic base metal. The CTOD tested specimens were examined by sectioning,

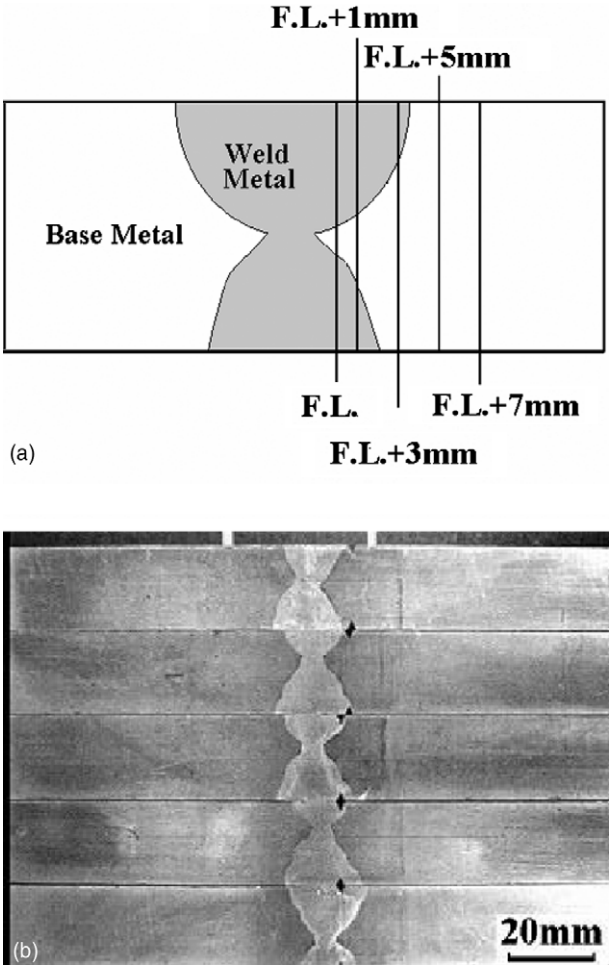

Fig. 2. Change in notch locations which is equivalent to side-groove locations in CCA specimens: (a) schematic diagram of the notch locations and (b) cross-sectional view of specimens with different side-groove locations.

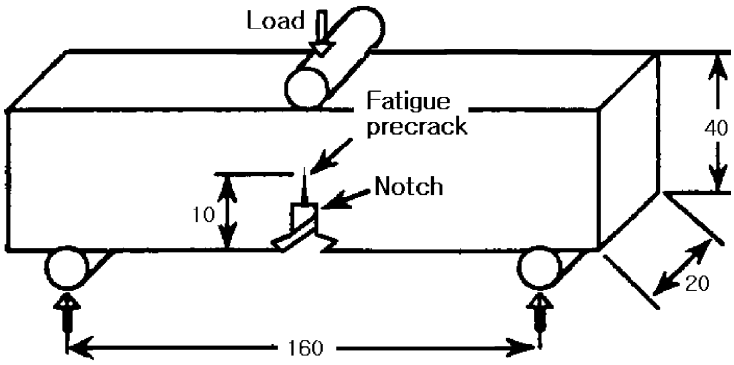

Fig. 3. Schematic illustration showing CTOD test setup and specimen geometry.

polishing and macroetching the sample sequentially to determine whether the precrack location and the crack initiation point were within the expected location or not. The sectioning was carried out in the manner recommended by API RP 2Z [7]. To verify the tendency of toughness changes seen in the CTOD tests, Charpy impact tests were additionally performed at low temperature. Standard 2 mm-V-notched specimens were taken from center of X-groove in the weld joints, and the notch positions from the fusion line are the same as in Fig. 2(a). In all toughness tests in this study including CCA tests, CTOD tests and Charpy impact tests, at least three toughness values were obtained under each condition, and it was the minimum value among them that was used to estimate the lower bound toughness.

3. Results and discussion

The results of the CTOD tests and Charpy impact tests for SA- and SMA-welded specimens at low temperatures are shown in Figs. 4 and 5, respectively. As expected, crack initiation fracture toughness, i.e., CTOD values, decreases as the precrack location approaches the fusion line from the base metal, which is attributable to the increase in the fraction of LBZ. The decreasing tendency is also seen in the results from Charpy impact tests. However, even the regions near the fusion line (FL) such as FL or FL + 1 mm show

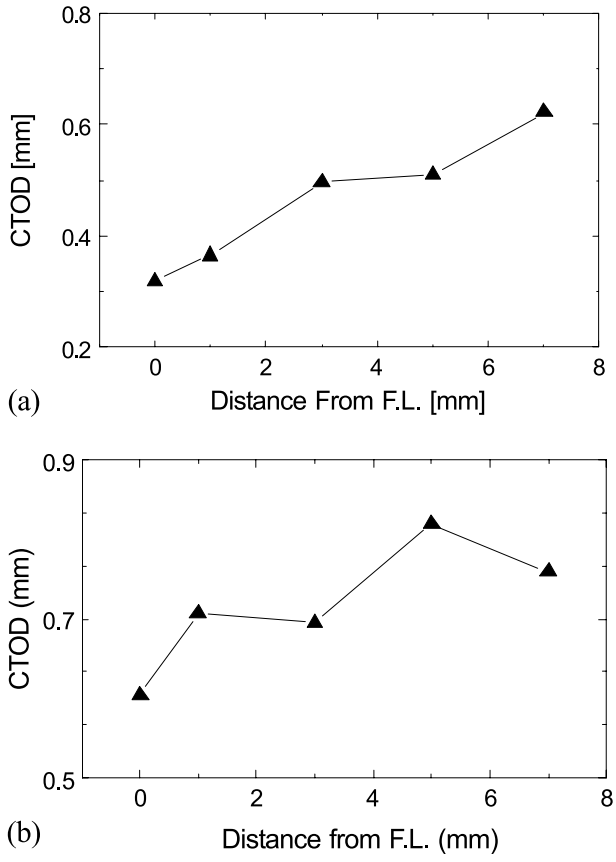

Fig. 4. Variations in CTOD values along the distance from the fusion line: (a) SMAW specimen and (b) SAW specimen.

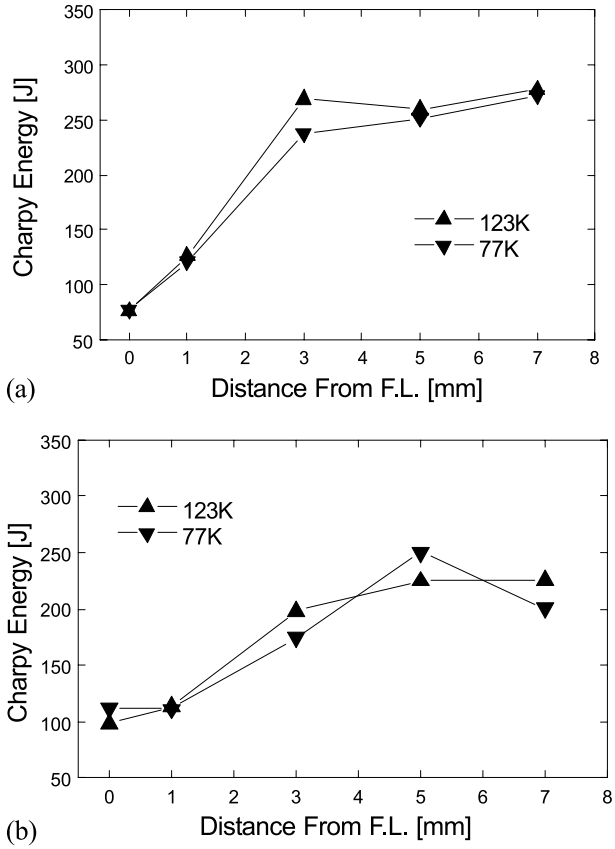

Fig. 5. Variations in Charpy impact values along the distance from the fusion line at low temperatures: (a) SMAW specimen and (b) SAW specimen.

the moderate values of both CTOD and impact energy. This result is interesting because the regions near the fusion line have large fraction of IC CGHAZ and UA CGHAZ, these zones being defined as the LBZs of this steel HAZs at cryogenic temperature, in authors' previous study [10]. Additionally, the presence of multiple load-drops in the load–displacement curves obtained from the CTOD tests for the specimens with precracks located near the fusion line is noticeable, as shown in Fig. 6. In the figure, the specimen for the fusion line shows many load-drops compared with the specimen for the FL + 3 mm. One of the microstructural differences between the FL and FL + 3 mm is presence of LBZs (IC CGHAZ and UA CGHAZ) in the former and their absence in the latter, and thus it can be known that the multiple load-drops observed in the specimens for the regions near fusion line are related to the existence of LBZs and to the crack arrest behavior, as described below.

The results of the CCA tests at 111 K are presented in Fig. 7. Unlike the CTOD test results, the crack arrest toughness values, K_a, at the regions between the FL and FL + 3 mm are much higher than those at FL + 5 mm and FL + 7 mm. These results are somewhat surprising because the regions near the fusion line have a larger LBZ fraction in their crack tips than that of the FL + 5 mm and +7 mm regions, these latter two regions being expected to have almost exactly similar mechanical properties to the base metal because of the relatively low peak temperature of the welding thermal cycle.

The different tendency of toughness between crack initiation and crack arrest can be explained by systematic observation of microstructure distribution within HAZ. An example of the representative

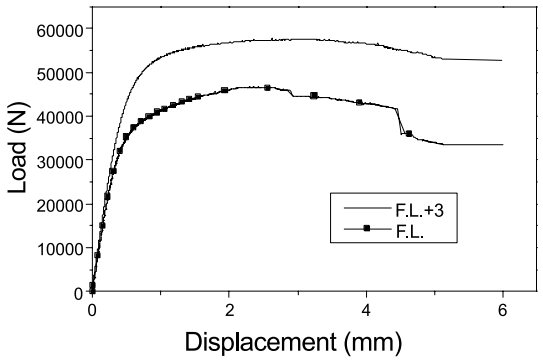

Fig. 6. Load–displacement curves obtained from CTOD tests using specimens precracked at fusion line (FL) and FL + 3 mm, respectively.

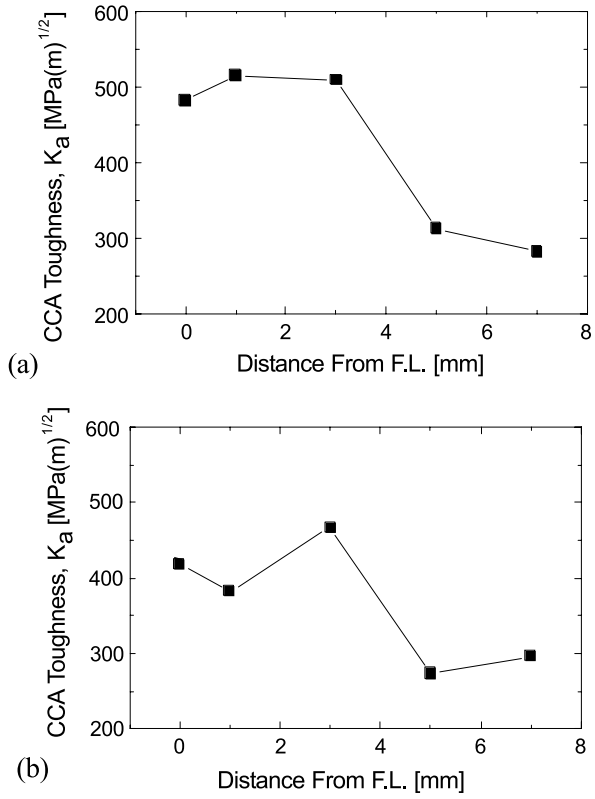

Fig. 7. Variations in crack arrestability along the distance from the fusion line: (a) SMAW specimen and (b) SAW specimens.

microstructure-distribution maps of the X-grooved weldments used in this study is shown in Fig. 8. The map was created by metallographic treatment of the weldment surface and by the consideration of the thermal cyclic history. The thermal cycle history is indicated based on the macroetched weldment using Eq. (1) for the thermal cycle range according to peak temperature [19,20].

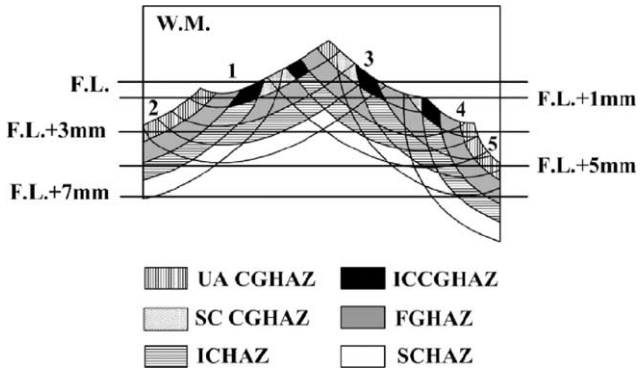

Fig. 8. An example of microstructure-distribution maps showing the change in fraction of subzones according to the notch locations.

$$\frac{r}{d_{\mathrm{HAZ}}} = \frac{\sqrt{(A_{\mathrm{C3}} - T_0)}}{\sqrt{(T_{\mathrm{p}} - T_0)}} \cdot \frac{\sqrt{(T_{\mathrm{mp}} - T_0)} - \sqrt{(T_{\mathrm{p}} - T_0)}}{\sqrt{(T_{\mathrm{mp}} - T_0)} - \sqrt{(A_{\mathrm{C3}} - T_0)}} \tag{1}$$

where r is the perpendicular distance from the fusion line to the region with peak temperature (T_{P}), T_{mp} is melting temperature, T_0 is inter-pass temperature, and d_{HAZ} is a distance between the fusion line and the HAZ line observed by macroetching and taken as the A_{C3} boundary. In this study, A_{C3} is 968 K, obtained from dilatometry test, T_{mp} is 1723 K, and T_0 is 383 K. In addition, 1323, 968, 823 and 723 K were used for T_{P} of the CGHAZs, fine-grained HAZs (FGHAZs) with recrystallized microstructures, inter-critical HAZ (ICHAZs) with partially transformed microstructures, and subcritical HAZs (SCHAZs) with tempered microstructures, respectively. A CGHAZ can be categorized again into four characteristic zones according to the peak temperature of subsequent thermal cycles in a multi-pass welding procedure: unaltered CGHAZ (UA CGHAZ), super-critically reheated CGHAZ (SCR CGHAZ) which is also treated as a FGHAZ, inter-critically reheated CGHAZ (IC CGHAZ), and subcritically reheated CGHAZ (SC CGHAZ). From a similar viewpoint, the microstructural classification listed in Table 2 was adopted in this investigation. In the map shown in Fig. 8, the line and the number indicate notch location and welding sequence, respectively. It can be seen from the map that the decrease in CTOD values near fusion line is due to the microstructures of possible LBZs, i.e., primarily IC CGHAZ and secondarily UA CGHAZ, are mainly identified at the fusion line (FL) or FL + 1 mm. In the case of crack arrest toughness, however, the main difference in microstructures between the high arrestability regions and the other regions is not the existence of LBZs but rather the large fraction of fine-grained HAZs (FGHAZs). By definition, FGHAZs have very fine grain size due to recrystallization during welding which results in their increased toughness relative to the base metal. Malik et al. [12] have suggested that crack arrest behavior is not a weakest-link-type event to be controlled by the most embrittled region such as LBZs, but rather a collective event which reflects the fracture toughness of the whole microstructures surrounding the crack initiation point. In a similar light, a comparison of the CCA test results with the microstructure-distribution map clearly indicates that the high crack arrestability near the fusion line is controlled by the rule-of-mixture of the microstructures in the crack tip front of the CCA specimens, and thus by the large fraction of FGHAZs irrespective of the presence of LBZs, although the fraction of LBZ at FL and FL + 1 mm is large enough to initiate a brittle crack.

Based upon the toughness values, practical influence of LBZ on brittle fracture resistance of this steel was investigated. Direct comparison of brittle crack initiation toughness (K_{c}) with brittle crack arrest toughness (K_{a}) is one of the easiest ways to determine whether brittle fracture has occurred or not. If K_{c} is higher than K_{a} and a brittle crack initiates, the crack cannot be arrested without propagation into a low

Table 2
Classification of microstructures in the HAZ in this study (specific temperatures are according to the steel used in this work)

Peak temperature of first cycle (T_{P1})	Peak temperature of subsequent cycle (T_{P2})	Microstructure of HAZ
Melting point–1323 K(CGHAZ)	Melting point–1323 K	UA CGHAZ
	1323 K–968 K (A_{C3})	SCR CGHAZ (= FGHAZ)
	968 K (A_{C3})–823 K (A_{C1})	IC CGHAZ
	823 K (A_{C1})–723 K	SC CGHAZ
	723 K–below	UA CGHAZ
1323 K–968 K (A_{C3})(FGHAZ)	Melting point–1323 K	UA CGHAZ
	1323 K–968 K (A_{C3})	FGHAZ
	968 K (A_{C3})–823 K (A_{C1})	ICHAZ
	823 K (A_{C1})–below	FGHAZ
968 K (A_{C3})–823 K (A_{C1})(ICHAZ)	Melting point–1323 K	UA CGHAZ
	1323 K–968 K (A_{C3})	FGHAZ
	968 K (A_{C3})–below	ICHAZ
823 K (A_{C1})–723 K or below(SCHAZ)	Melting point–1323 K	UA CGHAZ
	1323 K–968 K (A_{C3})	FGHAZ
	968 K (A_{C3})–823 K (A_{C1})	ICHAZ
	823 K (A_{C1})–below	SCHAZ

stress or high temperature region. Conversely, if K_a is higher than K_c, the initiated brittle crack can easily be arrested. In this case, the associated load-drops can also be observed in load–displacement curves during the toughness tests. So, the direct comparison of K_a with K_c is a very effective method to predict the practical risk level associated with the LBZ existence.

For direct comparison, firstly the thickness difference between the 20-mm-thick CTOD specimens and the CCA specimens with the same thickness but featuring 5-mm-deep side-grooves should be considered since fracture toughness increases with decreasing thickness. The Japanese standard WES-3003 [21] reports the correction method of K_a in accordance with thickness change, as Eqs. (2a)–(2c) for steels used at low temperature like the 9% Ni steel:

$$f(B) = 1 - \frac{1}{20}(B - 30) \quad \text{for} \quad B \leqslant 35 \text{ mm} \tag{2a}$$

$$f(B) = \frac{54}{65} - \frac{3B}{1300} \quad \text{for} \quad 35 \text{ mm} < B \leqslant 100 \text{ mm} \tag{2b}$$

$$K_a(B_1) = K_a(B_2)\frac{f(B_1)}{f(B_2)} \tag{2c}$$

where B is specimen thickness of mm dimension, and $K_a(B)$ is K_a value of the specimen with thickness of B. Eq. (2a) is for the specimen with thickness below 35 mm while Eq. (2b) for that over 35 mm. Machida et al. [22] applied this equation to QT-treated 9% Ni steel, and reported that they could predict successfully the toughness of the specimen with other thicknesses, as shown in Fig. 9 [22]. Similarly in this study, the crack arrest toughness values obtained from the specimens with side-grooves were corrected by the following correction ratio: $f(20)/f(15) = 1.5/1.75$. Fig. 10 shows the thickness-corrected value of K_a.

Next, the brittle crack initiation toughness represented by K_c needs to be extracted from the CTOD toughness. In many studies [12,22], Eq. (3) is generally used for this conversion:

$$K^2 = m\sigma_{YS}E\delta \tag{3}$$

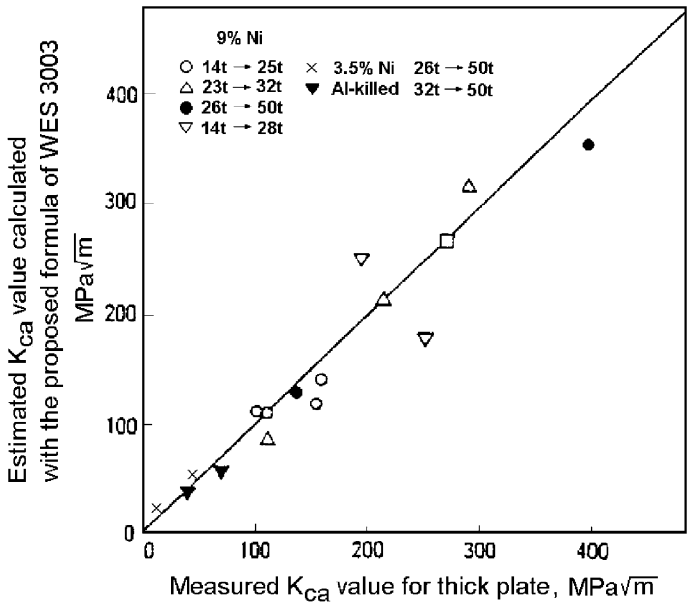

Fig. 9. The effect of plate thickness on K_a value of 9% Ni steel with the formula proposed in WES 3003, estimated by Machida et al. [22].

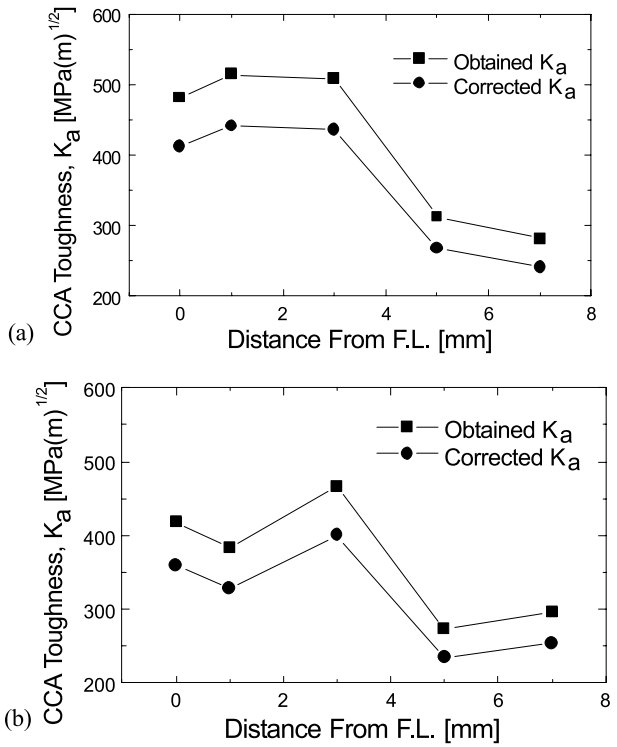

Fig. 10. Correction of thickness reduction due to side-groove in CCA specimen: (a) SMAW specimen and (b) SAW specimen.

where m is a dimensionless constant that is approximately 1 for plane stress condition and approximately 2 for plane strain condition, and where σ_{YS}, E and δ are yield strength, elastic modulus and CTOD, respectively. However, this relationship is available only when the obtained δ is δ_C (critical CTOD), because Eq. (3) is derived from the first term (δ_{el}) of Eq. (4):

$$\delta = \delta_{el} + \delta_{pl} = \frac{K^2(1-v^2)}{m\sigma_{YS}E} + \frac{r_P(W-a)}{r_P(W-a)+a}V_g \tag{4}$$

where δ_{el} and δ_{pl} are the elastic and the plastic terms of CTOD, respectively, and where the standard notifications in ASTM E1290 [15] are applied to the other symbols. As shown in Fig. 6, the CTOD values obtained in this study are δ_m (maximum CTOD) including both δ_{el} and δ_{pl}. So, Eq. (5), which considers the plastic term, is used for the conversion from CTOD values to K values.

$$K^2 = m\sigma_{YS}E\left(\frac{\delta}{2}\right) \tag{5}$$

In the equation, it is assumed that the elastic term is half of the total CTOD. Since the value of the elastic term is actually less than a tenth of the total CTOD value, the K_c value obtained is still an overestimated value, although using Eq. (5).

Fig. 11 shows the results of the direct comparison between the thickness-corrected value of K_a and the converted K_c. For all the regions, K_a is higher than K_c. Specifically, K_a is much higher than K_c near the

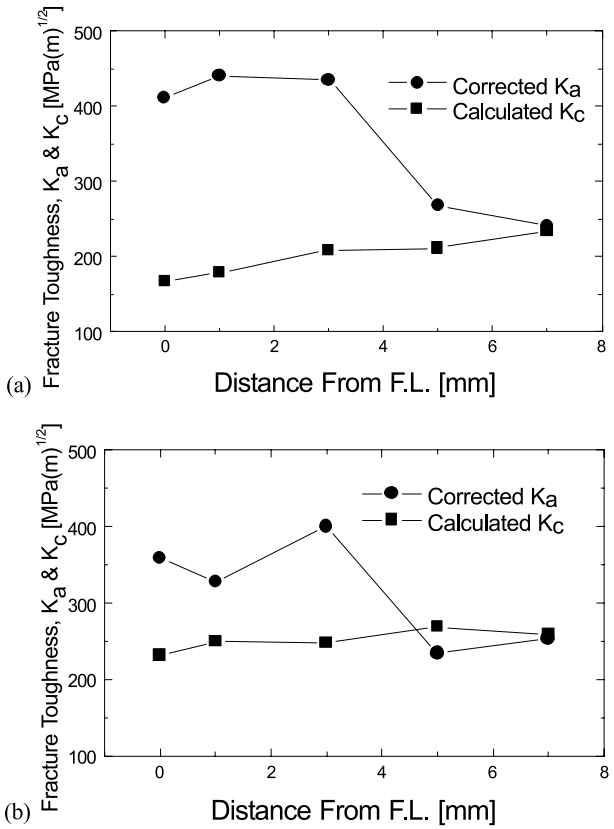

Fig. 11. Comparison of corrected K_a with K_c which was calculated by Eq. (5): (a) SMAW specimen and (b) SAW specimen.

fusion line where LBZs largely exist. Therefore, it is apparent that even if a brittle crack initiates at (or near) the LBZs, the crack will be easily arrested after only a short propagation distance.

From all the results obtained above, the crack arrest behavior of this steel HAZ at low temperature can be predicted as follows. When there is a through-thickness crack near the fusion line, the LBZs exist in the form of a continuous band along the direction of crack propagation. In this case, maintenance of a crack front through the thickness and continued propagation depend on the toughness of the material adjacent to the LBZs as well the LBZs themselves, indicating that, for the crack propagation featuring a uniform shape, the microstructures surrounding the LBZs should have similar toughness to that of the LBZs themselves. But, the regions including FGHAZ have much higher toughness than the LBZs, and these regions suppress the propagation of a brittle crack. Therefore, the initiated crack is arrested after a short propagation distance. The crack arrest behavior can be verified by the presence of multiple load-drops in the load–displacement curve obtained from the CTOD tests, as shown in Fig. 6. Conclusively, this investigation has determined that in regards to crack arrest behavior, LBZs of QLT-9% Ni steel may not limit the practical safety performance of the practical weldments in LNG storage tanks. The results also suggest that the conventional concept of LBZ effects based on crack initiation behavior can be somewhat over-conservative.

4. Conclusions

This study has investigated the practical influence of LBZs on the brittle fracture resistance of the weld HAZs in advanced 9% Ni steel, currently developed and used for large-scale LNG storage tanks, by observing the change in crack arrest toughness obtained from CCA tests and by comparing this change with the change in crack initiation toughness calculated from CTOD test results. In spite of the presence of LBZs near the fusion line, the crack arrest toughness values increases as the fusion line is approached, and the K_a values are much higher than those of K_c at the regions near the fusion line where LBZs largely exist. This finding is due to the fact that the observed crack arrest behavior is not a weakest-link-typed event controlled by the LBZs but rather a rule-of-mixture-typed event controlled by the microstructures surrounding the crack initiation points such as LBZs. Therefore, in the case of brittle crack initiation, such a crack will easily be arrested after propagating only a very short distance. From all the results of this study, it is concluded that LBZs of this steel may not represent a critical risk factor in the practical fracture performance of actual weldments in LNG storage tanks.

Acknowledgements

Authors are very grateful to Professor Masao Toyoda of Osaka University for his helpful discussion of this work.

References

[1] Fairchild DP. Fracture toughness testing of weld heat-affected zones in structural steel. Fatigue and Fracture Testing of Weldments, ASTM STP 1058. American Society for Testing and Materials, 1990. p. 117–41.
[2] Kim BC, Lee S, Kim NJ, Lee DY. Microstructure and local brittle zone phenomena in high-strength low-alloy steel. Metall Trans A 1991;22:139–49.
[3] Lee S, Kim BC, Kwon D. Correlation of microstructure and fracture properties in weld heat-affected zones of thermomechanically controlled processed steels. Metall Trans A 1992;23:2803–16.
[4] Toyoda M. Fracture strength of welded joints with mechanical heterogeneity. J Jpn Weld Soc 1990;59:166–72.

[5] Okada H, Matsuda F, Li Z. The behaviors of M-A constituent in simulated HAZ with single and multiple thermal cycles. Q J Jpn Weld Soc 1994;12:126–31.
[6] Davis CL, King JE. Cleavage initiation in the intercritically reheated coarse-grained heat-affected zone: part I. Fractographic evidence. Metall Trans A 1994;25:563–73.
[7] API RP 2Z. Recommended practice for preproduction qualification for steel plates for offshore structures, 2nd edition. American Petroleum Institute, 1992.
[8] EEMUA publication no. 150. Steel specification for fixed offshore structures, The Engineering Equipment and Materials Users Association, 1987.
[9] Lee CH, Lee SW, Yoo JY, Choo WY. Effects of heat treatment on the transformation and thermal stability of retained austenite in 9% Ni Steel. Proceedings of the Second Pacific Rim International Conference on Advanced Materials and Processing, Kyongju, Korea, 1995. p. 2035–44.
[10] Jang JI, Yang YC, Kim WS, Kwon D. A study on local brittle zone phenomena in cryogenic steel weldment. Proceedings of the 18th International Conference on OMAE, St. Jones, Canada, August, 1999; OMAE99/MAT-2419, published on CD-ROM.
[11] Jang JI, Ju JB, Kim WS, Kwon D. Influences of HAZ characteristics on CTOD toughness variation in multi-pass welded cryogenic steel. Proceedings of the International OMAE/ETCE joint conference: energy for the new millenium, New Orleans, Louisiana, USA, February 2000. OMAE2000/MAT-2110, published on CD-ROM.
[12] Malik L, Pussegoda LN, Gravile BA, Tyson WR. Crack arrest toughness of a heat-affected zone containing local brittle zones. J OMAE 1996;118:292–9.
[13] Kim JI, Syn CK, Morris Jr JW. Microstructural sources of toughness in QLT-treated 5.5 Ni cryogenic steel. Metall Trans A 1983;7:93–103.
[14] ASTM Standard E 1221. Standard test method for determining plane-strain crack arrest fracture toughness, K_{Ia}, of ferritic steel, American Society for Testing and Materials, 1988.
[15] ASTM Standard E 1290. Standard test method for crack-tip opening displacement (CTOD) fracture toughness measurement, American Society for Testing and Materials, 1993.
[16] British Standard 7448. Fracture mechanics toughness tests, Part 2: method for determination of K_{IC}, critical CTOD and critical J values of welds in metallic materials, British Standards Institution, 1997.
[17] Satoh K, Toyoda M, Minami F, Satoh S, Nakanishi M, Arimochi K. Crack tip plastic deformation of notched plates with mechanical heterogeneity. J Jpn Weld Soc 1983;52:154–61.
[18] Jang JI, Yang YC, Kim WS, Kwon D. A study of fracture toughness and microstructures in the weld heat-affected zone of QLT-processed 9% Ni steel. Adv Cryog Eng 1998;44:41–8.
[19] Nakao Y, Oshige H, Noi S. Distribution of microstructures in HAZ of multi-pass welded high strength steel. Q J Jpn Weld Soc 1985;3:766–73.
[20] Suzuki M, Bessyo K, Toyoda M, Minami F. Property distribution map to understand HAZ CTOD toughness. Q J Jpn Weld Soc 1995;13:302–8.
[21] WES Standard 3003. Evaluation criterion of rolled steels used for low temperature application, Japan Welding Engineering Society, 1983.
[22] Machida S, Ishikura N, Kubo N, Katayama N, Hagiwara Y, Arimochi K. Brittle fracture characteristics of heavy thickness 9% Ni steel plate and its application to large-scale LNG storage tanks. J High Pressure Inst Jpn 1991;29:25–39.